Experimental Spin Ratchet

Marius V. Costache, *et al.*

Science **330**, 1645 (2010);
DOI: 10.1126/science.1196228

Experimental Spin Ratchet

Marius V. Costache[1] and Sergio O. Valenzuela[1,2,3]*

Spintronics relies on the ability to transport and use the spin properties of an electron rather than its charge. We describe a spin ratchet at the single-electron level that produces spin currents with no net bias or charge transport. Our device is based on the ground-state energetics of a single-electron transistor comprising a superconducting island connected to normal leads via tunnel barriers with different resistances that break spatial symmetry. We demonstrate spin transport and quantify the spin ratchet efficiency by using ferromagnetic leads with known spin polarization. Our results are modeled theoretically and provide a robust route to the generation and manipulation of pure spin currents.

Brownian motors or ratchets refer to directed transport in the presence of a signal or perturbation that drives the system without an obvious bias in any preferred direction of motion. The perturbation generates useful work, for instance, the transport of particles, when combined with asymmetry, often realized by a so-called ratchet potential (Fig. 1A) (*1*–*3*). Experimental realizations of ratchets are spread over many different fields of biology, chemistry, and physics, where the perturbation may be external to the system (e.g., induced by an experimentalist) or intrinsic to it (e.g., nonthermal noise). In mesoscopic structures, experiments have demonstrated ratchets in both the quantum and classical limits (*4*–*6*). On such small scales, noise rectification with ratchets can be used to control particle transport and has become one of the most promising techniques for powering nanodevices (*3*).

Because of the growing interest in the spin degree of freedom as a carrier of information (*7*) as well as a means to address fundamental properties of quantum mechanics and quantum computation (*8*), a variety of ratchets have been proposed in pursuit of unidirectional spin currents and spin control (*9*–*12*). A pure spin ratchet (*11*) generalizes the particle ratchet mechanism (*1*–*3*), enabling pure spin currents by means of broken spatial symmetry (*9*–*12*). Thus, an indispensable hallmark for a spin ratchet is the breaking of the inversion symmetry for spin but not charge (*11*), whereby the ratchet-potential easy direction for one spin orientation is opposite to the ratchet-potential easy direction for the other spin orientation (Fig. 1A). Recent theoretical efforts use mesoscopic semiconductors and nonuniform magnetic fields (*9*), asymmetric periodic structures with Rashba spin-orbit interaction (*10*), and double-well structures combined with local external magnetic fields and resonant tunneling (*12*).

The concept of our spin ratchet is different from what has been proposed before. A small-volume superconducting (S) island is connected via tunnel junctions with two normal metal electrodes [N(l) and N(r)] to form an asymmetric single-electron transistor (SET) with different tunneling resistances (Fig. 1B). A voltage V applied across the SET drives the system, whereas a voltage on the back gate V_g sets the induced gate charge $Q = V_g C_g$ on the island, with C_g the capacitive coupling between the island and the gate.

At low temperatures, parity effects in the superconducting island are important (*13*–*16*). When the number of conduction electrons n is odd, there is necessarily one unpaired electron that is manifest as a quasiparticle excitation (*13*, *17*). The ground state energy of the system for odd n is higher than for even n by the superconducting gap Δ, which in our design is larger than the charging energy, E_c (Fig. 1C). In order to break the symmetry between spin-up and spin-down transport, a magnetic field B is applied in-plane along the axis of the electrodes [spin up refers to spins parallel to B, whereas spin down refers to spins antiparallel to B]. This field splits the quasiparticle levels (e.g., $n = 1^{\downarrow}$ and $n = 1^{\uparrow}$) by the Zeeman energy $E_Z = g\mu_B B$, where g is the g factor of the superconductor and μ_B the Bohr magneton, but it does not affect the Cooper-pair states (e.g., $n = 0$ and $n = 2$), which are singlet states, and it weakly reduces Δ because orbital depairing is minimized by an in-plane B (*18*) (Fig. 1, D and E). The $n = 1^{\downarrow}$ state shifts down continuously with increasing B and, at $B_{SR} = 2(\Delta - E_c)/(g\mu_B)$

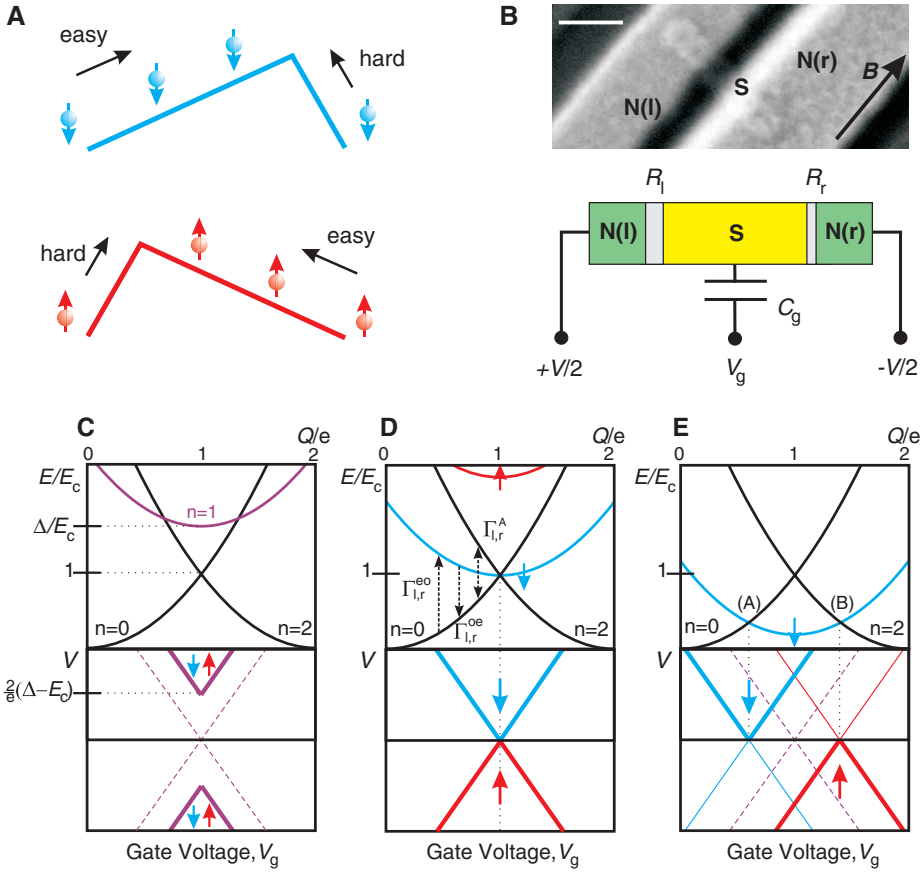

Fig. 1. SET spin ratchet. (**A**) In the presence of a ratchet potential and a driving force without a preferential direction, spin-down and spin-up electrons can be forced to move in opposite directions, giving rise to a spin current. (**B**) Scanning electron microscope image of an SET spin ratchet. A small-volume superconducting (S) island is contacted with two metal electrodes [N(l) and N(r)] via tunnel junctions with different tunnel resistances, $R_l > R_r$. The bar is 100 nm long. A voltage V is applied across the electrodes, and a voltage V_g on the back gate. (**C** to **E**) SET energetics of Cooper-pair and quasi-particle states (top) and associated below-gap voltage thresholds (bottom) for single- and two-electron transport at low temperatures for $B = 0$ (C), $B = B_{SR}$ (D) and $B > B_{SR}$ (E). Dashed and solid lines represent the positions of the Andreev and quasi-particle conductance thresholds, respectively.

[1]Institut Català de Nanotecnologia (ICN), Centre d'Investigació en Nanociència i Nanotecnologia (CIN2), Campus Universitat Autònoma de Barcelona, Bellaterra, Barcelona E-08913, Spain. [2]Institució Catalana de Recerca i Estudis Avançats (ICREA), Barcelona E-08010, Spain. [3]Department of Physics, Harvard University, Cambridge, MA 02138, USA.

*To whom correspondence should be addressed. E-mail: SOV@icrea.cat

(Fig. 1D), it becomes degenerate with both the zero ($n = 0$) and the one ($n = 2$) excess Cooper-pair states for $Q/e = 1$ (e is the electron charge).

The spin ratchet effect occurs at $B = B_{SR}$. Insight into the underlying mechanism can be gained by analyzing the relevant charge transport processes and their occurrence rates. Single-electron tunneling processes in the l and r junctions cause transitions between even (e) $n = 0,2$ and odd (o) $n = 1^{\downarrow}$ states with rates $\Gamma^{oe}_{l,r}$ and $\Gamma^{eo}_{l,r}$, whereas two-electron Andreev processes cause transitions between even $n = 0$ and $n = 2$ states with rates $\Gamma^{A}_{l,r}$ (Fig. 1D). For a spin ratchet, the rate hierarchy $\Gamma^{A}_{l,r} \ll \Gamma^{oe}_{l} < \Gamma^{oe}_{r} \ll \Gamma^{eo}_{l,r}$ is required, where the l junction transparency is chosen to be smaller than that of the r junction. There, driving single-particle cycles (subsequent addition and removal of an electron from the SET island) results in a net spin current into one preferred direction in the following manner. A cycle that only uses transitions between $n = 0$ and $n = 1^{\downarrow}$ (cycle 01) only transports spin-down electrons through the SET, whereas a cycle that only uses transitions between $n = 2$ and $n = 1^{\downarrow}$ (cycle 21) only transports spin-up electrons. The essential ingredient to the spin ratchet mechanism is that, for $\Gamma^{oe}_{l} < \Gamma^{oe}_{r}$, cycle 01 dominates at positive V, whereas cycle 21 dominates at negative V. Hence, in both cases there is a net spin-up current from, say, left to right through the SET. Because the charge transferred is null in average when a voltage V with zero mean is applied, the SET spin ratchet generates spin currents with no charge transport (*19*).

The thresholds for single- and two-electron Andreev events in an SET fulfilling the above rate hierarchy are shown schematically in Fig. 1, C, D, and E. At $B = 0$, single-electron transport sets in only for $V > 2(\Delta - E_c)/e$, when the odd state is reached ($Q/e = 1$). When B is applied, the Andreev and quasi-particle thresholds become closer, and, at B_{SR}, they coincide. There, single electron transport is possible even at $V \sim 0$, and the spin ratchet is effective for an unbiased V, where the spin orientation of moving electrons changes sign at $V = 0$. For larger B, the ground state energetics of the SET fully separates cycles 01 and 21 around the degeneracy points (A) and (B) (*18*). There, the asymmetric SET acts as a diode that resolves spin (*19*).

We have realized the proposed SET spin ratchet by using electron-beam lithography and shadow evaporation techniques (*20*). The small (6 nm thick by 40 nm wide by 250 nm long) superconducting island is made from aluminum, which is oxidized and contacted with two metal leads. Sequential deposition of the leads from two different angles allowed us to generate distinct tunneling resistances in the junctions (*19*). We verified the spin-ratchet mechanism in Fig. 1 by means of ferromagnetic (F) leads made of CoFe that were used as spin detectors (FSF device). The spin polarization sign change at $V = 0$ is preserved, as when using normal leads, but the effective polarization of the

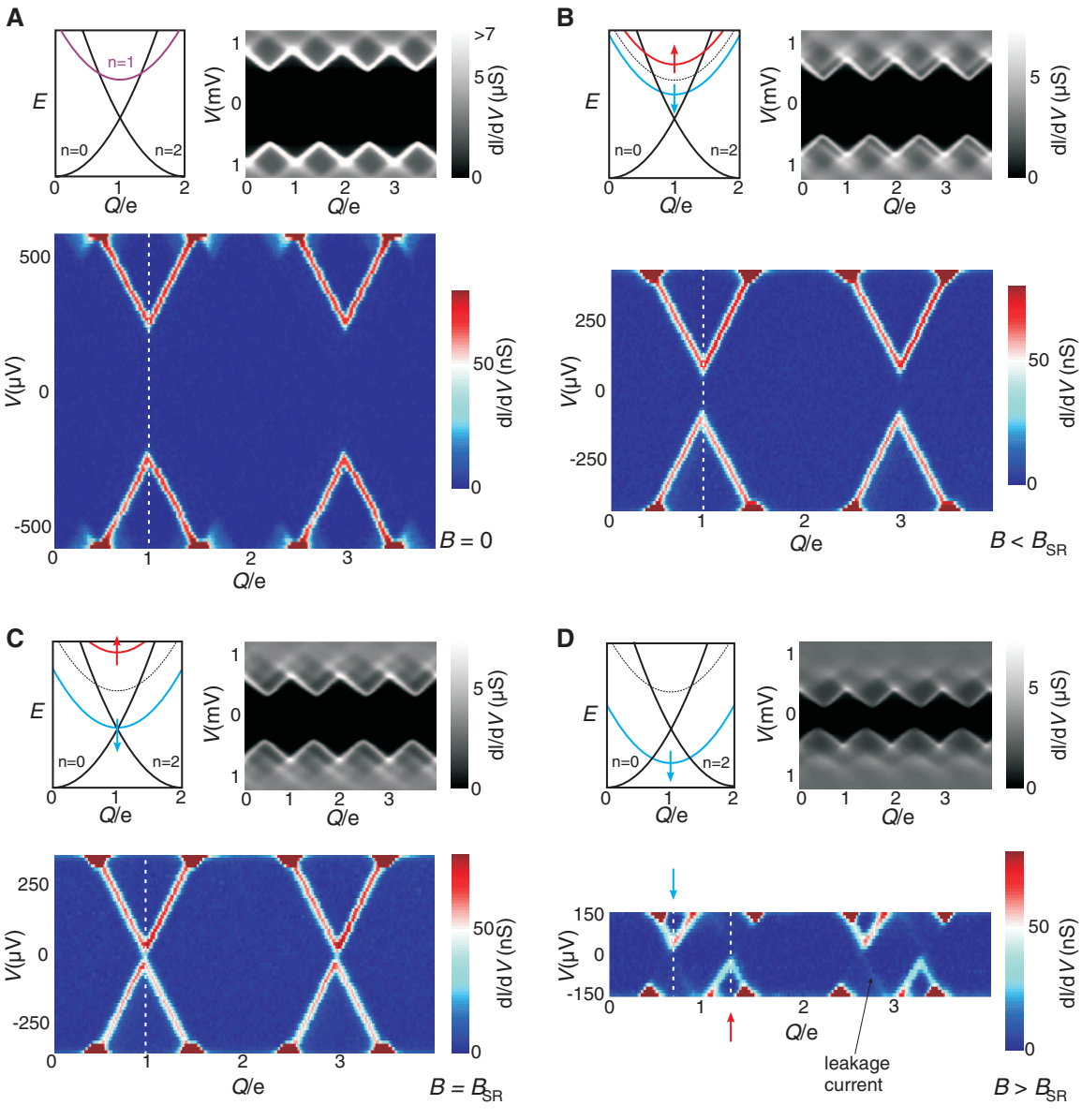

Fig. 2. Spin transport regimes in an applied magnetic field and characteristics of an SET spin ratchet. (**A**) $B = 0$. (**B**) $B = 1$ T. (**C**) $B = 1.5$ T. (**D**) $B = 2.5$ T. The top images represent the SET energetics of Copper-pair and quasi-particle states at the associated B (left) and show the above-gap response dI/dV versus V_g, which sets Q/e, and bias V (right). The bottom images show the below-gap transport in the SET (black area in the above-gap dI/dV plots), that is, dI/dV versus V_g, and bias V.

leads, P_F, measures the relative contribution of cycles 01 and 21. For a quantitative measurement of the spin-ratchet efficiency, we independently determined P_F. We accomplished this by using similarly fabricated junctions embedded in nonlocal spin devices, for which we obtained $P_F \sim 0.28$ (*20*, *21*).

The electron transport properties of such an FSF SET were fully characterized by means of differential conductance dI/dV measurements at above-gap voltage bias, from which we estimated $\Gamma_l^{oe} \approx 8 \times 10^6\ s^{-1} < \Gamma_r^{oe} \approx 4 \times 10^7\ s^{-1} << \Gamma_{l,r}^{eo} \approx 5 \times 10^9\ s^{-1}$ (*19*). Figure 2 shows the evolution of d*I*/d*V* as a function of the magnetic field at below-gap bias for this device. At $B = 0$, we observe a symmetric response about $V = 0$ (Fig. 2A). There, dI/dV is zero within the sensitivity of our measurements for voltage magnitudes below the gap, except at the quasi-particle thresholds, where it presents a peak whose intensity is nearly independent of V and V_g (*22*). The below-gap quasi-particle thresholds cross at about $V_0 = 259\ \mu V$ (Fig. 2A). This is in agreement with $V_0 \sim 2(\Delta - E_c)/e$ (Fig. 1C) when using $E_c = 170\ \mu eV$ and $\Delta \approx 303\ \mu eV$ as obtained from the above-gap thresholds [fig. S2 (*19*)]. At $B = 1$ T, V_0 decreases to 94 μV because of E_Z. At $B = 1.5$ T, V_0 becomes zero and the SET is in the pure spin ratchet regime (Fig. 1D) (*23*).

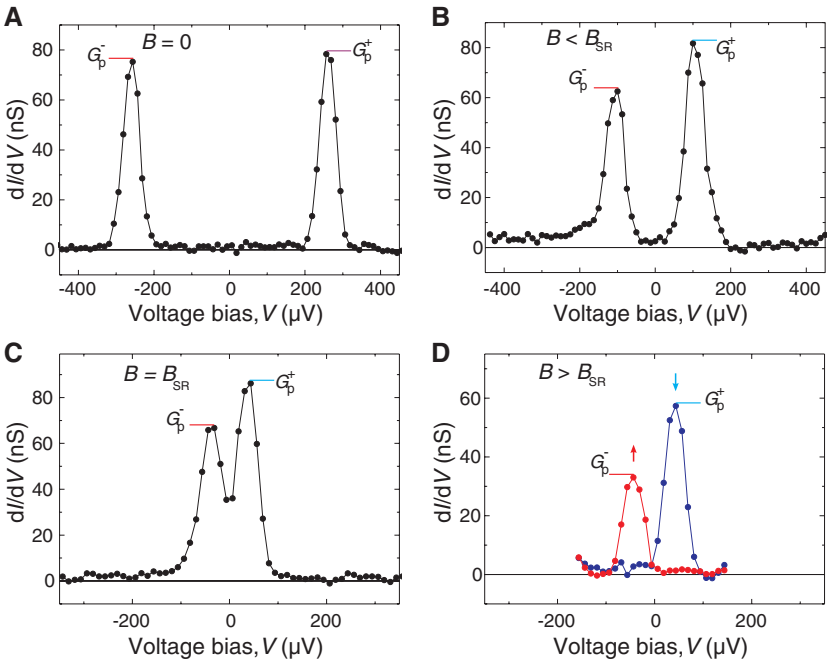

Fig. 3. Spin filtering. (**A**) $B = 0$. (**B**) $B = 1$ T. (**C**) $B = 1.5$ T. (**D**) $B = 2.5$ T. Differential conductance dI/dV versus V cross sections along the dotted white lines in Fig. 3. In (D), the red and blue curves are cross sections along the white lines indicated with red and blue, respectively, arrows in Fig. 2D.

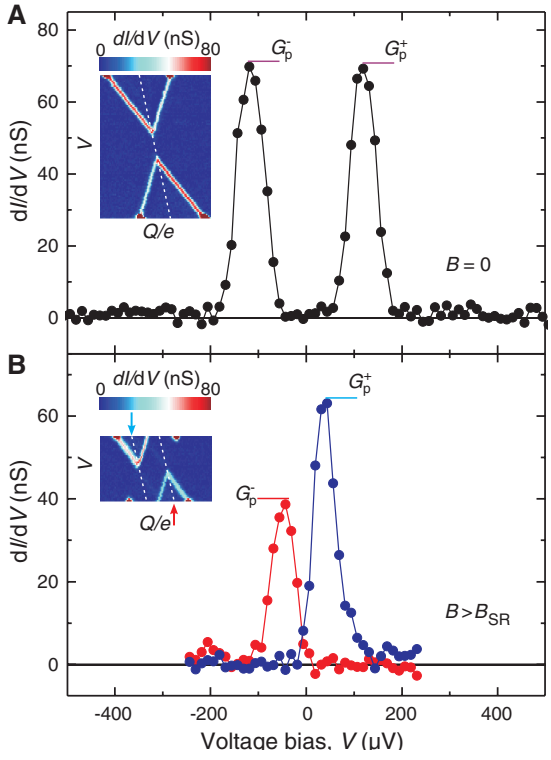

Fig. 4. Spin-filtering detection using an NSF sample. (**A**) $B = 0$. (**B**) $B = 2$ T. (Insets) dI/dV versus Q/e and bias V. The dI/dV versus V cross sections (main graphs) are taken along the corresponding dotted lines in the insets.

At magnetic fields $B > B_{SR}$, where the spin-up and spin-down quasi-particle thresholds are resolved, the SET behaves as a diode that filters spin-up or spin-down quasi-particles (Figs. 2D and 3D). Namely, the current should be polarized

Of key importance, the differential conductance at $B \neq 0$ (Fig. 2, B and C) is no longer symmetric about $V = 0$, presenting a larger magnitude for $V > 0$ than for $V < 0$ along the below-gap quasi-particle thresholds. This observation is consistent with the description in Fig. 1 and represents an experimental confirmation of the spin ratchet effect. Indeed, the asymmetry results from P_F and the fact that the current across the SET for positive and negative V has opposite spin polarization. The leads are always magnetized parallel to each other along the B direction and, because $P_F > 0$, they favor the dominant spin-down current cycle 01 at $V > 0$ and hinder the dominant spin-up current cycle 21 at $V < 0$. We quantify such a transport asymmetry by using the parameter $\beta = (G_p^+ - G_p^-)/(G_p^+ + G_p^-)$, where $G_p^+ = dI/dV\rfloor_{peak}$ $(V > 0)$ and $G_p^- = dI/dV\rfloor_{peak}$ $(V < 0)$ are the values of the peak conductances along the dotted white lines in Fig. 2. At $B = 0$ (Figs. 2A and 3A), β is zero within the sensitivity of our measurements, as expected. At $B = 1$ T and $B = 1.5$ T (Fig. 2, B and C, and Fig. 3, B and C), the difference between G_p^+ and G_p^- becomes apparent, resulting in $\beta \sim 0.14$ in both cases.

We define the spin-ratchet efficiency η_{SET} as equal to the spin-filtering capability $\eta_{SET} \approx (1 - \alpha)/(1 + \alpha)$ of our device, where the ratio $\alpha = \Gamma_l^{oe}/\Gamma_r^{oe} \approx R_r/R_l$ measures the asymmetry of the SET and $R_{l,r}$ are the associated normal tunnel resistance of junctions l and r (Fig. 1B). For $\alpha \sim 0$, nearly perfect filtering, that is, $\eta_{SET} \sim 1$, is achieved. In such a scenario, β directly measures the effective polarization of the leads; that is, $\beta = P_F = 0.28$. For $\alpha > 0$, a decrease in filtering efficiency is expected, and therefore β should decrease accordingly as $\beta \approx \eta_{SET} P_F$. For our device, $R_l \approx 350\ k\Omega$ and $R_r \approx 70\ k\Omega$ and $\alpha \sim 0.2$. We thus estimate $\eta_{SET} \sim 0.67$ and $\beta \approx \eta_{SET} P_F \sim 0.19$, a value that is somewhat larger than that obtained with our measurements ($\beta \sim 0.14$), which results in $\eta_{SET} \approx 0.5$. This discrepancy could be related to the uncertainty in the estimation of $R_{l,r}$ or to Andreev reflections in one of the junctions, which could contribute an unpolarized component to the total current.

fully spin-down for V_g about the degeneracy point (A) and fully spin-up for V_g about the degeneracy point (B) in Fig. 1E. Accordingly, we calculate β from the conductance peaks along the two dotted lines in Fig. 2D, obtaining β ~ 0.26, which is close to P_F ~ 0.28 and indicates a filtering efficiency larger than 0.9.

Lastly, we stress that the spin-ratchet effect is related to quasi-particle tunneling through the high-transparency junction (*22*). To further show this, we fabricated normal super conductor ferromagnet (NSF) devices with the normal metal lead made of Cu connected to the low-transparency junction. Here, $R_l \approx 650$ kΩ and $R_r \approx 70$ kΩ. Because the high-transparency tunnel barrier connected to the ferromagnetic lead controls the transport, β should remain close to P_F, when calculated as in Fig. 3D. Moreover, because R_r in this device is estimated to be of the same order of magnitude as that of the FSF device, the conductance peaks should not be substantially affected. Both these observations agree with the experimental *dI*/*dV* results shown in Fig. 4. At $B = 0$ (Fig. 4A), β is again zero within the sensitivity of our measurements and, at $B > B_{SR}$ (Fig. 4B), β ~ 0.25 ~ P_F, whereas the magnitudes of the conductance peaks compare well with those shown in Fig. 3.

Spin ratchets represent a fundamentally new approach for spin current generation and detection; thus, our research paves the way for a new means to study spin-related phenomena. Because the spin ratchets presented here work at the single-electron level, they can, for example, be used to initialize and read out the state of spin-based quantum bits (*8*) or to identify the spin orientation of single electrons in a test of the Einstein-Podolsky-Rosen paradox (*24*) with spin-entangled electrons (*25*–*29*).

References and Notes

1. P. Hänggi, F. Marchesoni, F. Nori, *Ann. Phys.* **14**, 51 (2005).
2. P. Reimann, *Phys. Rep.* **361**, 57 (2002).
3. P. Hänggi, F. Marchesoni, *Rev. Mod. Phys.* **81**, 387 (2009).
4. A. M. Song *et al.*, *Phys. Rev. Lett.* **80**, 3831 (1998).
5. H. Linke *et al.*, *Science* **286**, 2314 (1999).
6. J. E. Villegas *et al.*, *Science* **302**, 1188 (2003).
7. I. Žutić, J. Fabian, S. Das Sarma, *Rev. Mod. Phys.* **76**, 323 (2004).
8. D. D. Awschalom, D. Loss, N. Samarth, *Semiconductor Spintronics and Quantum Computation* (Springer-Verlag, Berlin, 2002).
9. M. Scheid, D. Bercioux, K. Richter, *N. J. Phys.* **9**, 401 (2007).
10. S. Smirnov, D. Bercioux, M. Grifoni, K. Richter, *Phys. Rev. Lett.* **100**, 230601 (2008).
11. M. E. Flatté, *Nat. Phys.* **4**, 587 (2008).
12. M. Scheid, A. Lassl, K. Richter, *EPL* **87**, 17001 (2009).
13. D. V. Averin, Y. V. Nazarov, *Phys. Rev. Lett.* **69**, 1993 (1992).
14. M. T. Tuominen, J. M. Hergenrother, T. S. Tighe, M. Tinkham, *Phys. Rev. Lett.* **69**, 1997 (1992).
15. T. M. Eiles, J. M. Martinis, M. H. Devoret, *Phys. Rev. Lett.* **70**, 1862 (1993).
16. F. W. J. Hekking, L. I. Glazman, K. A. Matveev, R. I. Shekhter, *Phys. Rev. Lett.* **70**, 4138 (1993).
17. G. Schön, in *Quantum Transport and Dissipation*, T. Dittrich *et al.*, Eds. (Wiley, Weinheim, Germany, 1998), chap. 3.
18. A. J. Ferguson, S. E. Andresen, R. Brenner, R. G. Clark, *Phys. Rev. Lett.* **97**, 086602 (2006).
19. Materials and methods are available as supporting material on *Science* Online.
20. S. O. Valenzuela, M. Tinkham, *Nature* **442**, 176 (2006).
21. S. O. Valenzuela, *Int. J. Mod. Phys. B* **23**, 2413 (2009).
22. A zero *dI*/*dV* below the quasi-particle thresholds suggests that the Andreev cycle (Fig. 1C) and cotunneling processes (*13*) are suppressed. Integration of *dI*/*dV* results in a current plateau I_p ~ 5.8 pA beyond the thresholds. Because the current is limited by Γ_r^{oe}, $I_p \approx e\Gamma_r^{oe}$ ~ 5 pA, which is in reasonable agreement with the measured value. This indicates that transport is dominated by tunneling events in the r junction.
23. The decrease in V_0 with increasing B is larger than expected if only E_Z is considered; in which case, the ratchet effect should occur at $B_{SR} \approx 2.3$ T. This is due to a reduction of Δ by residual orbital depairing. When such a reduction is considered, Δ(1 T) = 272 μeV, V_0(1 T) = $2[\Delta(1\text{ T}) - E_c]/e - E_Z/e \approx 88$ μV is close to the measured value. Moreover, considering Δ(1.5 T) = 256 μeV, we estimate $B_{SR} = [\Delta(1.5\text{ T}) - E_c]/(g\mu_B) \approx 1.48$ T, in agreement with the observed result.
24. A. Einstein, B. Podolsky, N. Rosen, *Phys. Rev.* **47**, 777 (1935).
25. C. Bena, S. Vishveshwara, L. Balents, M. P. A. Fisher, *Phys. Rev. Lett.* **89**, 037901 (2002).
26. D. S. Saraga, D. Loss, *Phys. Rev. Lett.* **90**, 166803 (2003).
27. L. Hofstetter, S. Csonka, J. Nygård, C. Schönenberger, *Nature* **461**, 960 (2009).
28. P. Cadden-Zimansky, J. Wei, V. Chandrasekhar, *Nat. Phys.* **5**, 393 (2009).
29. L. G. Herrmann *et al.*, *Phys. Rev. Lett.* **104**, 026801 (2010).

30. We gratefully acknowledge discussions with and support from M. Tinkham and thank I. Žutić and Y. Tserkovnyak for discussions and W. D. Oliver, P. Gambardella, and A. Bachtold for a critical reading of the manuscript. This research was supported in part by the Spanish Ministerio de Ciencia e Innovación (MAT2010-18065, FIS2009-06671-E). Samples were made at the Center for Nanoscale Systems, Harvard University.

Supporting Online Material

www.sciencemag.org/cgi/content/full/330/6011/1645/DC1
Materials and Methods
SOM Text
Figs. S1 to S3
References

9 August 2010; accepted 9 November 2010
10.1126/science.1196228

Spin Transfer Torques in MnSi at Ultralow Current Densities

F. Jonietz,[1] S. Mühlbauer,[1,2] C. Pfleiderer,[1]* A. Neubauer,[1] W. Münzer,[1] A. Bauer,[1] T. Adams,[1] R. Georgii,[1,2] P. Böni,[1] R. A. Duine,[3] K. Everschor,[4] M. Garst,[4] A. Rosch[4]

Spin manipulation using electric currents is one of the most promising directions in the field of spintronics. We used neutron scattering to observe the influence of an electric current on the magnetic structure in a bulk material. In the skyrmion lattice of manganese silicon, where the spins form a lattice of magnetic vortices similar to the vortex lattice in type II superconductors, we observe the rotation of the diffraction pattern in response to currents that are over five orders of magnitude smaller than those typically applied in experimental studies on current-driven magnetization dynamics in nanostructures. We attribute our observations to an extremely efficient coupling of inhomogeneous spin currents to topologically stable knots in spin structures.

The discovery of the effect of giant magnetoresistance, now used commercially in the hard disk drive industry, is widely recognized as the starting point of the field of spintronics. It represents the first example of electric currents controlled efficiently by spin structures. The complementary process of so-called spin transfer torques, where magnetic structures and textures are manipulated by electric currents (*1*, *2*), appears to be even more promising. For instance, strong current pulses allow the movement of ferromagnetic domain walls (*3*, *4*), the switching of magnetic domains in multilayer devices (*5*, *6*), the induction of microwave oscillations in nanomagnets (*7*), and the switching of ferromagnetic semiconductor structures (*8*). However, the typical current densities required to create observable spin transfer torques in present-day studies exceed 10^{11} A m^{-2}. Because this implies extreme ohmic heating, it was generally believed that spin torque effects can be studied exclusively in nanostructures. We report the observation of spin transfer torques in a bulk material, the skyrmion lattice phase of MnSi. The spin transfer torques appear when the current density exceeds an ultralow threshold of ~10^6 A m^{-2}, five orders of magnitude smaller than those used typically in experimental studies on current-driven magnetization dynamics in ferromagnetic metals and semiconductors.

The skyrmion lattice in chiral magnets, like MnSi and related B20 compounds, was only recently discovered in neutron-scattering studies (*9*–*12*) and confirmed to exist in Lorentz force microscopy for $Fe_{1-x}Co_xSi$ (x = 0.5) (*13*). It represents a new form of magnetic order that may be viewed as a crystallization of topologically stable knots of the spin structure that shares remarkable similarities with the mixed state in type II superconductors. For zero magnetic field (Fig. 1A), helimagnetic order appears in MnSi below the critical temperature T_c = 29.5 K.

[1]Physik-Department E21, Technische Universität München, D-85748 Garching, Germany. [2]Forschungsneutronenquelle Heinz Maier-Leibnitz (FRM II), Technische Universität München, D-85748 Garching, Germany. [3]Institute for Theoretical Physics, Utrecht University, 3584 CE Utrecht, Netherlands. [4]Institute of Theoretical Physics, University of Cologne, D-50937 Cologne, Germany.

*To whom correspondence should be addressed. E-mail: christian.pfleiderer@frm2.tum.de